# Computational Simulation Study of the influence of Faujasite Si/Al ratio on CO_2 capture by Temperature Swing Adsorption

Hèctor Prats, Daniel Bahamon, Xavier Giménez, Pablo Gamallo*
and Ramón Sayós

Departament de Ciència de Materials i Química Física & Institut de Química Teòrica i Computacional (IQTCUB), Universitat de Barcelona, C. Martí i Franquès 1, 08028 Barcelona, Spain.
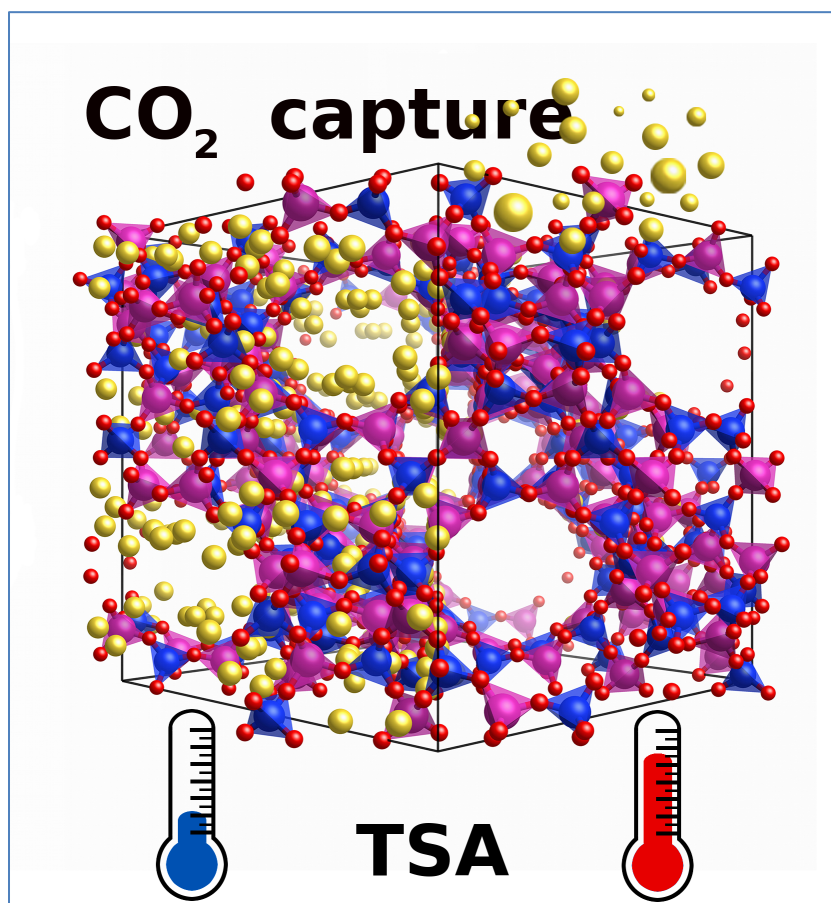
(graphical abstract)

*Corresponding author: *E-mail address: gamallo@ub.edu*
Postal address: Departament de Ciència de Materials i Química Física & Institut de Química Teòrica i Computacional (IQTCUB), Universitat de Barcelona, C. Martí i Franquès 1, 08028 Barcelona, Spain.

Abstract

Grand Canonical Monte–Carlo simulations are used to assess ten faujasite structures, the well–known family of zeolites with different Al content in post-combustion CO_2 capture via Temperature Swing Adsorption (TSA) processes, at 313-473 K and 100 kPa. Selectivity, working capacity, regenerability, purity, isosteric heat and working capacity values, for each structure, have been calculated from simulations, providing a rather complete evaluation of adsorbents' performance. Additionally, for all the structures the temperature dependence of the heat capacity has been modeled to estimate the thermal regeneration energy. Calculated heat capacities range from 0.78-0.86 kJ/kg·K at 313K to 0.98-1.15 kJ/kg·K at 473K, values considerably lower than those corresponding to aqueous amine solutions. Comparison of TSA results with previous Vacuum and Pressure Swing Adsorption (VSA and PSA) ones shows that there is no structure that works well for all three processes. Instead, each process reaches optimum conditions for certain range of Al content. Results indicate that high Al content faujasites, 64-to-96-FAU, are the most effective for TSA with working capacities above 1.7 mol/kg, doubling PSA/VSA values. Intermediate Al content 48-,64-FAU perform better at VSA conditions and low Al content 12-,24-FAU structures are more suitable for PSA processes. At moderate operative conditions (i.e., regeneration temperature of 413 K), TSA shows the highest purities (above 99% for one-stage process), followed by VSA and PSA. Finally, TSA is more effective in cleaning faujasites with 48 or more Al, compared to PSA/VSA, leading to a higher regenerability (energetic cost index range between 2.3-2.4 GJ/tCO_2).

Keywords: Zeolites; CO_2 Capture; GCMC; Faujasite; TSA

1. Introduction

Economic growth and industrial development have resulted in an increased burning of fossil fuels, leading to growing emissions of atmospheric CO_2 [1]. These emissions may be reduced by a variety of measures, such as improving energy efficiency, and/or developing alternative energy sources, e.g. wind and solar power. However, the necessary transition into a sustainable energy mix, and the phasing out of fossil fuel combustion, is unlikely to occur at a sufficiently fast pace, unless additional, negative emission methods are considered.

Reduction of energy-related CO_2 emissions might be undertaken by means of Carbon Capture and Sequestration/Utilization (CCS/U) techniques. In CCS/U, carbon dioxide is separated from the flue gas of a power plant, compressed to supercritical conditions to transport it, and either stored or reused as a raw material in industry[2,3,4,5,6].

Separation technologies with proven adequacy for post-combustion processes are absorption, membrane use, and adsorption.[7] Whereas the membrane technology is currently waiting its application to mass production, absorption is more mature, but it results in high-energy consumption during the absorbent regeneration step[8] (*i.e.*, about 30% of the output of the power plant).[9] Alternatively, CO_2 can be captured through adsorption in the pores of solid materials [10,11]. Adsorption technology is based on the preferential affinity of CO_2 to the adsorbent pores, compared to other flue gas components. After the adsorption step, molecules are desorbed from the solid by lowering the pressure (Pressure Swing Adsorption, PSA) or heating the solid material (Temperature Swing Adsorption, TSA) inside the column. The PSA process in which the desorption is performed below atmospheric pressure is called Vacuum Swing Adsorption (VSA). After this operation, the adsorbent is ready for a further cycle. All these methods have been used successfully for air fractionation, hydrogen production, carbon dioxide capture (CCS/U) and removal of volatile organic compounds (VOC) [12,13,14,15,16,17,18]. Among these methods, TSA is particularly promising, owing to difficulties with compressing or applying a vacuum to such large volumes of gas stream, as well as to the potential availability of low-grade heat in a power plant as a source of energy for regeneration [19].

Zeolites, activated carbons and metal−organic frameworks (MOFs) are promising adsorption materials, presenting high CO_2 working capacity and selectivity for CO_2 over N_2, together with low regeneration energy [10,20,21,22,23,24,25]. In particular, zeolites are inexpensive porous materials that are already produced on a large scale for many commercial applications. Thus, they have been used successfully in PSA and TSA processes for CCS/U [26,27,28]. Furthermore, they present higher thermal and mechanical stability than other common adsorbents such as MOFs, although the latest often possess higher surface areas [29,30].

Zeolites are molecular sieves with a 3D framework structure possessing orderly distributed micropores with diameters up to 2 nm. The different ways in which TO_4 tetrahedrals (T = Si or Al atom) can be connected lead to a rich variety of zeolite structures [31,32,33]. Faujasites are a zeolite family built from Si, Al and O atoms, with a crystal composition that vary with the Si/Al ratio (*i.e.*, $(Na_2O)_{n/2}(Al_2O_3)_{n/2}(SiO_2)_{192-n}$, $0 \leq n \leq 96$) [34], and consist of sodalite cages which are connected through hexagonal prisms. The properties of the faujasites depend on the nature, number and distribution of the framework cations. As the Si/Al ratio decreases, the cation content increases, the thermal stability diminishes, the surface becomes more hydrophilic and the zeolite increases its catalytic properties. These changes are of great importance in the energetic cost of the CO_2 capture and in the regenerability of the adsorbent material [35]. Thus, the open three-dimensional pore system of FAU-type zeolites allows exceptional properties for using it in adsorptive separations compared to other zeolite families [36].

Computational methods have been employed in a complementary fashion to experimental investigations. Grand-canonical Monte Carlo (GCMC) simulations allow the prediction of adsorption isotherms, adsorption selectivities and preferred adsorption sites at a very moderate computational expense, making an important contribution to the microscopic understanding of gas adsorption and separation in porous materials [37]. In a previous work [38], we have employed GCMC simulations to study the separation of post-combustion $CO_2/N_2/O_2$ mixtures via PSA and VSA processes in FAU-type zeolites with different Si/Al ratio. An analysis of the influence of the Si/Al ratio on the CO_2 capture performance revealed that faujasites having intermediate Al content are the most effective for P/VSA processes. In the present work, we have performed new GCMC simulations for

all faujasite structures considered in Ref. [38] to study the separation of post-combustion $CO_2/N_2/O_2$ mixtures via TSA processes. Thus, we have calculated selectivities, working capacities and purities at TSA conditions and then, compared the results obtained with those for PSA and VSA processes. Moreover, we have calculated the thermal regeneration energy (*i.e.,* the energy required for heating and desorb) and compare it with the adiabatic work for expansion/compression required in VSA/PSA processes.

This document is structured as follows: Section 2 describes the methodology, the computational details and the evaluation criteria used to rank all the faujasite structures simulated. Section 3 reports the values for all the properties calculated and gives the comparison of TSA versus PSA and VSA processes. Finally, Section 4 provides the main conclusions obtained.

2. Methods and computational details

2.1 Faujasite structures

Ten different Si/Al Faujasite structures have been studied in the present work. Since the full set of Faujasite structures are the same that those used in our previous work [38], here only a few details are given. These structures have been labeled as *n*–FAU, where *n* signifies the number of sodium or aluminum atoms per unit cell (*i.e.*, *n* = 0, 6, 12, 24, 32, 48, 64, 77, 88 and 96, which correspond to Si/Al ratio of +∞, 31, 15, 7, 5, 3, 2, 1.5, 1.2 and 1, respectively). All the structures were obtained from 88-FAU (*i.e.*, also named zeolite 13X), by randomly replacing Al by Si atoms and satisfying the Löwenstein's avoidance rule [39].

We considered all faujasites under study as rigid models. Nevertheless, the non-framework sodium cations were allowed to move freely along the zeolite structure, changing their position depending on their interactions within the rigid structure, other Na^+ cations and the adsorbed gas molecules, as recommended in previous studies [40,41].

2.2 Force field and simulation details

Carbon dioxide, nitrogen and oxygen molecules were modelled rigid. The potential of the system was calculated as the sum of the guest-host and the guest-guest interaction energies, modeled as a combination of Lennard-Jones (LJ 12-6) and Coulomb potentials

$$U_{ij} = 4\varepsilon_{ij}\left[\left(\frac{\sigma_{ij}}{r_{ij}}\right)^{12} - \left(\frac{\sigma_{ij}}{r_{ij}}\right)^{6}\right] + \frac{1}{4\pi\varepsilon_0}\frac{q_i q_j}{r_{ij}} \qquad (1)$$

where U_{ij} is the total potential energy between atoms i and j at distance r_{ij}; q_i, q_j are the partial charges of atoms i and j, respectively, ε_{ij} is the LJ potential well depth, σ_{ij} is the LJ potential diameter, and finally ε_0 is the vacuum permittivity. All the force field parameters were taken from Calero *et al.* [42,43]. These parameters are applicable to all Si/Al ratios, both at cryogenic and high temperatures.

Ewald summation was used to calculate Coulombic interactions [44] with a relative precision of 10^{-6}. A cutoff distance of 12 Å was used, and Lorentz-Berthelot mixing rules were used to calculate the van der Waals interactions between molecules. A summary of the Coulombic charges and LJ parameters used in this work, as well as the agreement between simulations and experimental data for selected structures (when available), can be found in the Supplementary data from our previous study [38].

Pure and ternary mixture adsorption isobars were computed using GCMC simulations by means of LAMMPS code [44]. At every simulation step, the GCMC algorithm attempts a number of insertions/deletions of guest molecules between the simulation cell and the imaginary reservoir, and a number of translations/rotations of guest molecules within the simulation box. Simulations have been run for at least 4×10^6 GCMC equilibration steps and 8×10^6 GCMC production steps for each temperature value. The number of molecules adsorbed was calculated using a statistically averaged approach after the equilibrium stage for every single point, allowing the construction of the adsorption isobars [45].

Both pure and ternary mixture isobars were computed at a pressure of 1 bar, in a temperature range between 313 and 473 K. The separation efficiency of the ternary mixture $CO_2/N_2/O_2$ was studied, with a typical post-combustion gas composition of 15%/80%/5% [46] (*i.e.*, we assume that water and other impurities have been removed from the tail gas in earlier stages).

To relate the chemical potential with the pressure in the present simulations the Peng-Robinson Equation of State (EOS) [47] was used, taking the pure substance parameters from NIST database [48]. The van der Waals one-fluid mixing rule was used in mixture simulations [49], taking the binary parameters from Vrabec *et al.* [50]. Additional details regarding the GCMC simulations and force-field parameters can be found in our previous work [38].

2.3. Adsorbent evaluation criteria

Five different evaluation criteria were considered in this work to analyze the CO_2 capture and separation performance for each faujasite under the studied conditions: selectivity (s_{CO_2/N_2}), CO_2 working capacity (WC_{CO_2}), regenerability (R_{CO_2}), purity at outlet (X_{CO_2}) and thermal regeneration energy ($Q_{thermal}$). All of them can be obtained, respectively, from the following expressions:

$$s_{CO_2/N_2} = \left(\frac{x_{CO_2}}{x_{N_2}}\right) \Big/ \left(\frac{y_{CO_2}}{y_{N_2}}\right) \tag{2}$$

$$WC_{CO_2} = N_{CO_2}^{ads} - \phi N_{CO_2}^{des} \tag{3}$$

$$R_{CO_2} = \left(WC_{CO_2}/N_{CO_2}^{ads}\right) \times 100\% \tag{4}$$

$$X_{CO_2} = \frac{N_{CO_2}^{out}}{N_{gas}^{out}} = \frac{\dfrac{P_{CO_2}V\epsilon}{RT} + WC_{CO_2}\rho V(1-\epsilon)}{\dfrac{P_{TOT}V\epsilon}{RT} + \left(WC_{CO_2} + WC_{N_2} + WC_{O_2}\right)\rho V(1-\epsilon)} \tag{5}$$

$$Q_{thermal} = \int_{T_{des}}^{T_{ads}} C_p^{FAU} dT + \sum_k q_{ST_k} WC_k \qquad (6)$$

where x_i is the molar fraction of i-component in the adsorbed phase and y_i is the molar fraction of i-component in the bulk/gas phase, and WC_{CO_2} is calculated from the difference between the CO_2 uptake under adsorption and desorption conditions per kg of adsorbent material and per cycle. The usual procedure of estimating the working capacity experimentally in TSA processes [51] consists in calculating $N_{CO_2}^{ads}$ from ternary mixture adsorption data and $N_{CO_2}^{des}$ from pure CO_2 adsorption data. However, this procedure assumes that after adsorption step the composition inside the bed is 100% CO_2, which is only valid for high selective materials, as in Ref. [51]. However, faujasites structures with low Al content (*i.e.,* 0-FAU to 24-FAU) also contain a non-negligible fraction of N_2 and O_2 molecules adsorbed. Thus, for these structures, at desorption conditions the value of $N_{CO_2}^{des}$ which has been calculated from pure CO_2 adsorption data at 100 kPa must be corrected because P_{TOT} does not equal P_{CO_2}. The correction is done by the ϕ factor [38] that varies between 0 and 1 and considers the molar fraction x_{CO_2} in the adsorbed phase, providing a more realistic method of estimating the number of molecules that will remain adsorbed after the desorption step. As above-mentioned, this approach is necessary for low Al content structures where other uptakes are not negligible, and it makes results more realistic than those found in the literature based on pure adsorption data [14,52], which are only valid when the material is highly selective for one component. The values of ϕ used in this study correspond to 1.00, 0.99, 0.99, 0.98, 0.96, 0.93, 0.87, 0.75, 0.54 and 0.44 for n-FAU structures with $n=$ 96, 88, 77, 64, 48, 32, 24, 12, 6 and 0, respectively.

Regeneration of CO_2, Eq. (4), represents the fraction in percentage of carbon dioxide that can be desorbed by heating up the adsorbent material from the total uptake of gas species. On the other hand, the CO_2 purity at the outlet of the bed, Eq. (5), is an important variable to consider, especially when is possible to reuse the captured CO_2 for other applications. In Eq. (5), the ratio $N_{CO_2}^{out}/N_{gas}^{out}$ indicates the molar fraction of CO_2 in the mixture exiting the adsorbent material. This ratio is calculated considering the void

fraction of the bed (*i.e.,* the ratio of the void volume to the total volume of the bed), $\epsilon = 0.4$, the feed composition, $P_{CO_2} = 15$ kPa and $P_{TOT} = 100$ kPa, the volume of the packed bed, $V = 0.1$ m³, the working capacity of component i at desorption temperature T, WC_i and the framework density, ρ.

The total thermal regeneration energy ($Q_{thermal}$) per unit mass of adsorbent has two main contributions: (i) the energy required for heating the adsorbent material, and (ii) the energy required to overcome the endothermic desorption process. According to Sculley et al., [53] this energy can be calculated per kg of adsorbent in one cycle from Eq. (6) where C_p^{FAU} is the heat capacity of the adsorbent, T_{ads} and T_{des} are the adsorption and desorption temperatures, respectively and finally, q_{ST_k} and WC_k are the isosteric heat of adsorption and working capacity of k-component in the mixture, respectively. q_{ST_k} is a thermodynamic quantity that characterizes the enthalpy change associated with the adsorption of one molecule onto the surface. According to the energy/particle fluctuations in the GC ensemble, the isosteric heat of adsorption (q_{st_k}) corresponds to [54]:

$$q_{st_k} = -\frac{\langle U \times N \rangle - \langle U \rangle \langle N \rangle}{\langle N^2 \rangle - \langle N \rangle^2} + \langle U_g \rangle + RT \qquad (7)$$

where U is the total potential energy of the N adsorbed molecules and the brackets $\langle ... \rangle$ denote an average in the GC ensemble. The bracket terms have been obtained from GCMC simulations by averaging over 10.000 different values for each loading. Moreover, we have assumed that the isosteric heat remains constant throughout the desorption step at the value corresponding to the adsorption uptake. This is a good approximation due to the flatness of the isosteric heat curves as a function of the CO₂ uptake (Fig. 1). Finally, $\langle U_g \rangle$ is the average energy of an isolated adsorbate molecule in the ideal-gas state. For rigid molecules, this term vanishes.

On the other hand, C_P is an important parameter for the energy requirements calculation, since materials with low heat capacity would lead to lower energy penalties for the regeneration step, Eq. (6). Unfortunately, only a limited number of specific heat capacities have already been measured and reported in literature for cation-exchanged faujasites [55,56,57]. In the present work, heat capacities for all the structures have been computed by means of the predictive model from Vieillard [58], based on the oxide

summation technique. This method considers that the thermodynamic properties of silicate minerals can be described as a linear combination of the fractional properties of their constituent polyhedral, where only the crystallography of the mineral needs to be known. The C_P value of our FAU structures were calculated in the following way:

$$C_p^{FAU}(T) = n_{SiO_2} \cdot C_p^{SiO_2}(T) + n_{Al_2O_3} \cdot C_p^{Al_2O_3}(T) + n_{Na_2O} \cdot C_p^{Na_2O}(T) \qquad (8)$$

where C_p^i are the heat capacities of the i-polyhedral, n_i is the total number of i-polyhedrals present in a unit cell, and the $C_p^i(T)$ values are obtained from a polynomial correlation with temperature. Calculated heat capacities range from 0.78-0.86 kJ/kg·K at 313 K to 0.98-1.15 kJ/kg·K at 473 K. Interestingly, there is a nearly linear relationship between the heat capacity and temperature for all the faujasite structures (see Fig. S1 in Supplementary data). These values of $C_p^i(T)$ are considerably lower than those conventionally employed in aqueous amine solutions since the presence of water in which the amine molecules are dissolved must also be heated until desorption temperature. For example, the heat capacity for 30% wt monoethanolamine (MEA) solution at 298 K is 3.73 kJ/kg·K, more than four times larger[59]. These results highlight one of the main advantages of employing zeolites or other porous solid materials such as MOFs when TSA process is adopted. Details regarding the heat capacity calculation can be found in Section I of the Supplementary data.

In the present work, we consider TSA processes in their simplest configuration including only two fixed beds in parallel by the so-called Skarstrom cycle [60]. When comparing among the different faujasite structures, both the total volume of the column and the fractional voidage were held constant, implying that the volumes of adsorbent materials used in the fixed beds are equal for all faujasite structures.

Moreover, it needs to be mentioned that the different adsorption criteria used in the present work should be used with caution when aiming to predict the best material for post-combustion CO_2 capture. Our results provide key insights regarding the performance of different faujasites structures, but they must always be accompanied by kinetic studies under realistic process conditions. In fact, there have been a few works investigating the capability of adsorbent metrics to screen potential adsorbents. [61,62] These studies

indicated that adsorbent criteria could identify the adsorbents that eventually performed poorly. However, the relative ranking provided by various metrics can be different.

3. Results and discussion

3.1. Isosteric heat of adsorption

Isosteric heat of adsorption (q_{st}) is an important thermodynamic quantity for understanding the possible thermal effects related to adsorption. It can be used to compare the interaction strength of the adsorbates with various adsorbent materials. The isosteric heats of adsorption at different CO_2 uptakes for the different faujasite structures analyzed in this work are plotted in Fig. 1.

The isosteric heats of adsorption of CO_2 at zero coverage increase from 14 to 42 kJ·mol^{-1} from the pure silica zeolite (with a Si/Al ratio of $+\infty$) to the 96-FAU zeolite (with a Si/Al ratio of 1), respectively. This fact comes from the increasing number of strong interactions between Na$^+$ cations and gas molecules from 0-FAU to 96-FAU structures. This tendency is also observed for CO_2 uptakes up to 5 mol/kg. Above this loading value, different adsorption behaviors start to appear, especially for faujasites with a high Al content.
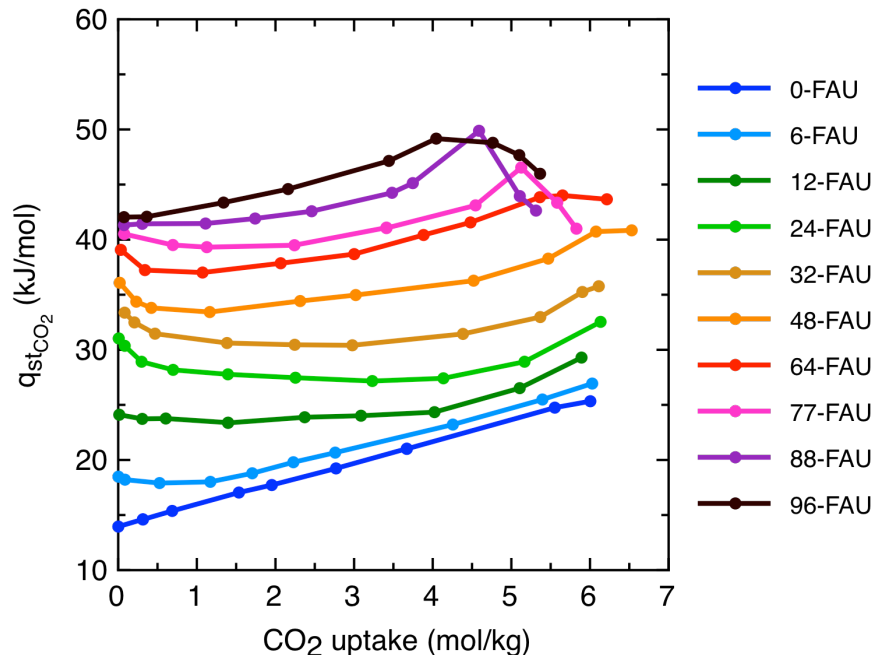
Figure 1. Isosteric heat of adsorption (q_{st,CO_2}) as a function of the CO_2 uptake per kg of adsorbent material obtained for the ten faujasite structures with different Si/Al ratio at T=313 K. Lines are guide to the eye.

The flatness of the isosteric heat curves observed for intermediate Al content faujasites (*i.e.,* from 12-FAU to 64-FAU) indicates that solid-gas interactions are dominant along the whole adsorption process until high loadings. Conversely, the increase of the adsorption heat with the loading for low Al content faujasites (*i.e.*, 0-FAU and 6-FAU) suggests that the adsorption regime at low CO_2 coverage is dominated by solid-gas interactions, while this interaction becomes less important as the CO_2 loading increases due to the formation of new gas-gas interactions, which are stronger. However, high Al content structures (from 77-FAU to 96-FAU) show a different behavior and the heat of adsorption decreases upon reaching a certain value. Above this value, the CO_2 molecules and the Na^+ cations are so close together that the gas-gas and Na^+-gas interactions become more repulsive (*i.e.*, the structure reaches saturation). Fig. 1 shows that 96-FAU structure is the one that presents the isosteric heat decay at a lower loading, since it contains a higher number of Na^+ cations than the other structures. A similar behavior has been reported previously for LTA

structures with different Si/Al ratios [28]. The values of the isosteric heat at different loadings will be used to calculate the thermal regeneration energy.

3.2. Selectivity, purity and regenerability

Fig. 2 shows the selectivity for CO_2 relative to N_2 for the ten structures evaluated as a function of temperature according to Eq. (2). As expected, 96-FAU has the highest CO_2 selectivity in all the temperatures considered, ranging from 1150 (313K) to 46 (473K), while 0-FAU has the lowest value, between 4.1-2.1 in the same temperature range. This is due to the strong interactions between CO_2 and Na^+ cations and the increasing value of the isosteric heat of adsorption, which are dominant in structures with high Al content. Moreover, as the thermal energy of the gas molecules increases, the difference in adsorption between CO_2 and N_2 becomes less significant, so decreasing the selectivity. The drop in selectivity with temperature is more pronounced for structures with higher selectivity (*e.g.*, a factor of 25 for 96-FAU compared to a factor of 2 for 0-FAU in the same temperature range). The fact that systems with large selectivity are more sensitive to temperature has been observed also in MOFs [63].

Selectivity values in Fig. 2 have been obtained directly from ternary mixture isotherms obtained from GCMC simulations. In addition, selectivity has been also evaluated using adsorption isotherm fits for pure components followed by IAST calculations (Fig. S4 in Supplementary data). Selectivity values obtained from IAST calculations are substantially larger than those values obtained directly from ternary mixture isotherms, specially for low Al-content faujasites, as reported previously in Ref. [38] since IAST does not consider the interaction among all the species in the mixture, as GCMC does.
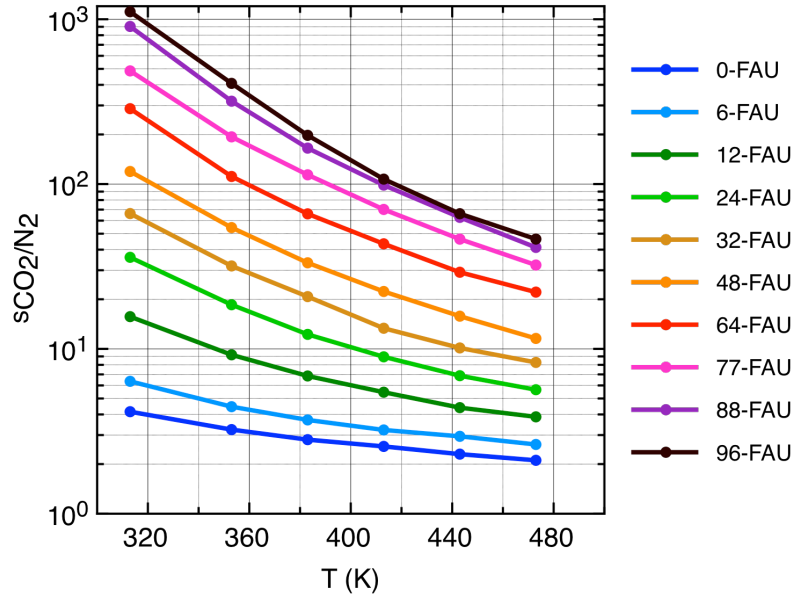
Figure 2. Calculated selectivities for CO_2 relative to N_2 as a function of temperature, for ten different n-FAU structures (P_{TOT} = 100 kPa).

Fig. 3 shows calculated values of CO_2 purity at outlet and regenerability as a function of desorption temperature for all the faujasite structures, assuming a packed bed with a total volume of 0.1 m³ (*i.e.,* L = 0.1 m, A = 1 m²) and a void fraction of ϵ = 0.4. The highest purities are obtained for high Al-content structures, with values above 90% for structures containing more than 48 Na⁺ atoms per unit cell. This degree of purity agrees with real feed experimental value of 94% of purity at outlet obtained in Ref. [18] for 13X (FAU-88) performing TSA processes with a smaller amount of CO_2 (10%) and a bit different operative conditions (T_{ads} = 288 K, T_{des} = 423 K). Purity values corresponding to 77-FAU, 88-FAU and 96-FAU structures are coincident, and therefore they cannot be distinguished in the plot. Conversely, purity values for 0-FAU, 6-FAU and 12-FAU structures are very low, making them not attractive for the process. Note that the final CO_2 purity depends on the selectivity, the working capacities for $CO_2/N_2/O_2$, and on the void fraction ϵ. Higher purity values can be achieved by reducing the void fraction.
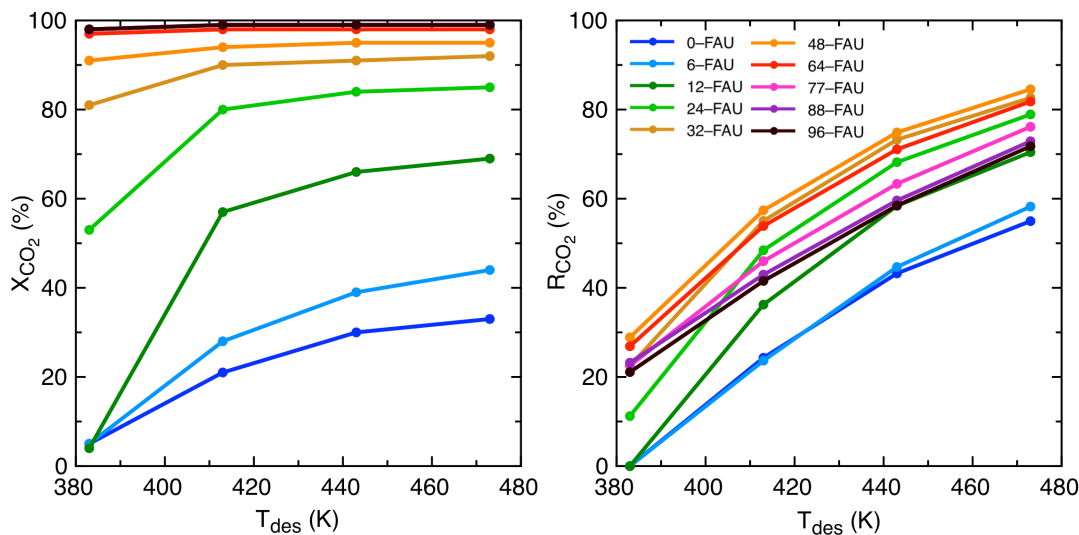
Figure 3. CO_2 purity at outlet (%) in the gaseous mixture exiting the bed (left) and regenerability (right) as function of desorption temperature, assuming a packed bed with a total volume of 0.1 m³ (L = 0.1 m, A = 1 m²) and a void fraction of ϵ = 0.4. Simulations performed at T_{ads} = 313 K and P_{TOT} = 100 kPa.

Unlike purity, maximum regenerability values are obtained for intermediate Al content structures, with 48-FAU having the highest value at all temperatures explored. Even though, it should be noted that although certain structures such as 12-FAU and 24-FAU present moderately high regenerability, their uptake is so low that the amount of recovered CO_2, in absolute terms, is small. It can be expected that regenerability will be even higher at temperatures above 473K. Purity and regenerability values corresponding to lower desorption temperatures have not been plotted in Fig. 3, since the working capacity at these conditions is nearly zero for most of the structures, and hence the CO_2 purity and regenerability tend to 15% and 0%, respectively.

Pure adsorption isobars for CO_2 and ternary mixture isobars for CO_2 and N_2 can be found in Section II and Section III in the Supplementary data, respectively.

3.3. Working capacity, thermal regeneration energy and optimal desorption temperature

Desorption temperature can significantly affect both the CO_2 working capacity and the thermal regeneration energy, which are the two main parameters to study the performance of the adsorbent materials for carbon capture and sequestration [53]. Fig. 4 shows the variations of these two quantities as a function of desorption temperature in the range 353-473 K.

As it can be seen in Fig. 4a, the working capacity initially increases quickly with increasing temperature and then nearly reaches a plateau for most of the structures. The initial sharp increase can be attributed to the fact that the influence of temperature on the gas/solid interactions is more remarkable at low temperatures [63], and can be also deduced from the shape of the CO_2 adsorption isobars (see Section III in the Supplementary data). Low and intermediate Al content structures reach the plateau at temperature values around 473 K, whereas for high Al content structures this plateau is beyond the temperature range considered in the present work.
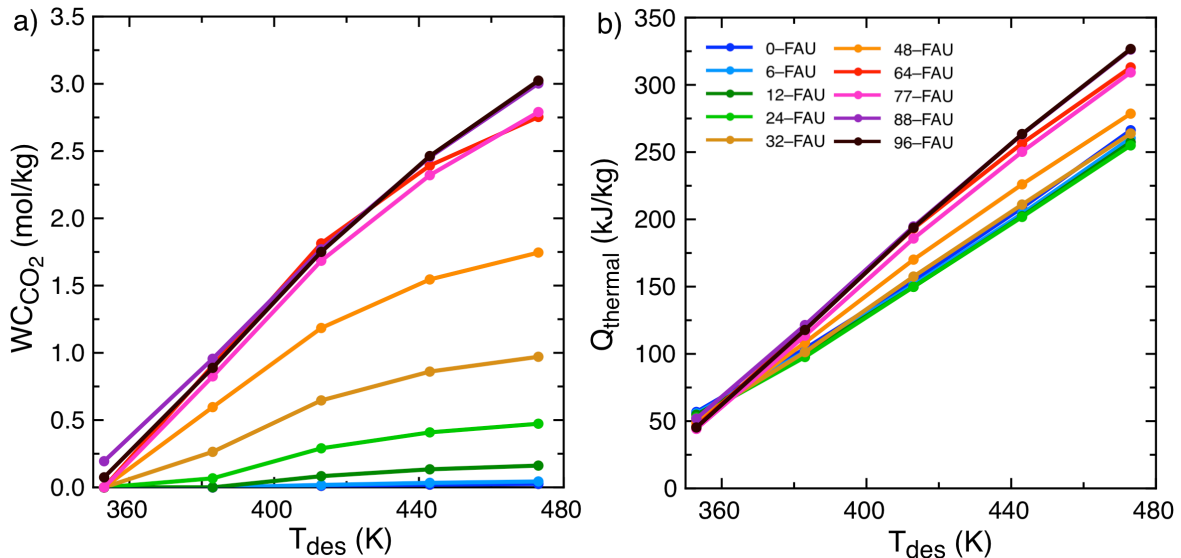

Figure 4. Influence of TSA desorption temperature on the CO_2 working capacity (a) and required thermal regeneration energy (b) for the different faujasite structures (T_{ads} = 313 K, CO_2 (15%), N_2 (80%), O_2 (5%) and P_{TOT} = 100 kPa). WC_{CO_2} and $Q_{thermal}$ values plotted are per cycle.

Table 1. Mass and volumetric working capacity values per cycle for selected faujasite structures from this work and other promising adsorbents found in literature. The temperature range considered is T_{ads} = 313 K – T_{des} = 443 K and P_{TOT}=100 kPa for all the materials except for en-M(dobpdc) MOFs. [a,b] Values for X-FAU structures correspond to a ternary CO_2 (15%)/N_2(80%)/O_2(5%) mixture, whereas the other values correspond to a binary CO_2(15%)/N_2(85%) mixture.

Material	Working capacity		Ref.
	(mol/kg)	(mol/dm^3)	
64-FAU	2.40	3.20	this work
88-FAU	2.45	3.41	this work
96-FAU	2.46	3.47	this work
CaX	2.20	3.14	[61]
MgX	2.37	3.38	[61]
PS-MFI	0.36	0.67	[61]
CaA	2.79	4.22	[51]
CuBTC	0.88	0.84	[61]
Ni-MOF-74	1.71	2.05	[61]
Zn-MOF-74	1.13	1.38	[61]
Mg-MOF-74	4.25	3.36	[14]
ZIF-68	0.21	0.19	[61]
PPN-6-SO$_3$Li	0.62	0.32	[53]
PPN-6-SO$_3$H	0.36	0.12	[53]
en-Mg$_2$(dobpdc) [a]	0.60	0.52	[64]
mmen-Mg$_2$(dobpdc) [b]	3.60	3.13	[65]
mmen-Mn$_2$(dobpdc) [b]	2.80	2.35	[65]

[a] temperature range: T_{ads} = 298 K – T_{des} = 423 K.

[b] temperature range: T_{ads} = 313 K – T_{des} = 413 K.

In post-combustion CO_2 capture, the solid adsorbent will likely be packed into a large fixed bed, and, as such, the volumetric working capacity in units of mol/dm^3 is also a vital consideration from the perspective of minimizing the size of the column towers, which may affect the heating efficiency during the regeneration step. Alternatively, the bed porosity or void fraction (ϵ = 0.4) could be used to estimate the bed densities and use those

values to obtain a volumetric working capacity values that are related to the size of the fixed beds. For the faujasite structures considered in the present work, both mass capacity and volumetric capacity analysis lead to the same ranking due to their similar density. However, when comparing between different materials, a volumetric capacity ranking is more useful. Framework density was used to convert from mass-specific to volume-specific working capacity. Table 1 compares our results for mass capacity and volumetric capacity with those for promising adsorbent materials found in literature. We found that high Al-content faujasite structures have competitive capacity values beating the vast majority of the other zeolites and being only surpassed in volumetric capacity by zeolite CaA, although it presents a higher heat of adsorption of 58 kJ/mol[51], which may imply more energy required to overcome the endothermic desorption process. In the case of MOFs, some of them also present higher working capacities. To name a few, Mg-MOF-74 [14] and mmen-Mg$_2$(dobpdc) [65] present higher mass capacity and similar volumetric capacity than high Al-content faujasites at T_{ads} = 313 K – T_{des} = 443 K, 413 K, respectively. Additionally, it is important to note that experimental materials are not fully activated and then some discrepancies could appear in their performance compared to simulated perfect crystals. Moreover, small temperature changes can occur during the adsorption and desorption steps due to the exothermic and endothermic processes that take place, respectively.

In contrast, Fig. 4b shows that there is a nearly linear relationship between the required thermal regeneration energy per cycle and the desorption temperature. This fact can be explained analyzing both terms in Eq. (6) separately. Both terms increase with temperature, however, the first one increases in a concave manner while the second increases in a convex manner, resulting in a total increase that is almost constant with temperature.

To seek out the optimal desorption temperature, both contributions should be considered. Hence, by calculating the required thermal regeneration energy per unit mass of CO$_2$ recovered as a function of desorption temperature (presented in Fig. 5) it is possible to estimate the optimal desorption temperature. According to Sculley et al. [53], this simplest ratio will be the most telling, as it will give a true direct comparison between materials, independent of assumptions about the process. Of course, the values obtained in GJ/kg do not represent the real cost for the whole capture process. There are other factors that will

come into play during the industrial process, such as the efficiency of types of heat exchangers, capital costs of equipment and adsorbent materials and costs associated to post-separation (*e.g.,* compression and transport), among others.
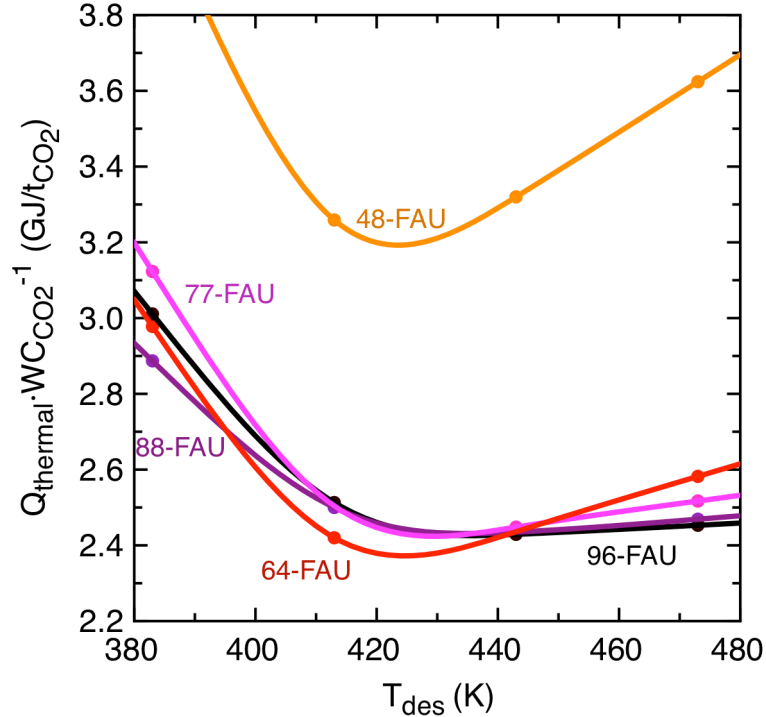

Figure 5. Thermal regeneration energy per ton of CO_2 recovered as a function of desorption temperature at P_{TOT} = 100 kPa. Lines are guide to the eyes.

Fig. 5 shows that the optimum desorption temperature is between 413 and 443 K. In addition, it can be observed that TSA process is only profitable for faujasites with more than 48 Al atoms per unit cell. The low working capacity for structures with lower Al content does not compensate their lower heat capacity. Moreover, the values obtained for 64-, 77-, 88- and 96-FAU structures are very similar in all the temperature range considered. This is due to similar values of density, heat capacity, isosteric heat and working capacity. Among these structures, 64-FAU has the minimum thermal regeneration energy per unit mass of CO_2 recovered at 413 K, with a value of 2.42 GJ/tCO_2. This value is in line with the real feed experimental value of 2.02 GJ/tCO_2 reported in Ref. [17] using PTSA at operative conditions T_{ads} = 323 K – T_{des} = 373 K, at pressures 15% below atmospheric conditions, with 11.5% of CO_2 at feeding and using CaX zeolites (same as

19

FAU-88 with Ca^{2+} instead of Na^+ cations). On the other hand, Ref. [18] reports a real feed value of 8.8 GJ/tCO$_2$ for TSA, FAU-88 although for 10% of CO_2 in the incoming mixture. This value is higher than that obtained here but they operated at larger range of temperatures T_{ads} = 288 K – T_{des} = 423 K. As they stated the adiabatic estimate of the thermal regeneration energy halves the previous value to 4.4 GJ/tCO$_2$.

Finally, flue gas can be used directly from the stack stream to pre-heat the bed at the desorption step, allowing to reduce the regeneration thermal energy for the process [66]. For instance, assuming a stack temperature of 400 K, a reduction of 10% could be achieved.

3.4. Comparison of TSA separation performance versus PSA and VSA processes

In Sections 3.2 and 3.3 we have shown that the best faujasite structures to be used in TSA processes for post-combustion CO_2 capture are those with a higher Al content, from 64-FAU to 96-FAU. These structures stand out in all the five different evaluation criteria considered, especially when the temperature of desorption is raised between 413 and 473 K. In order to determine whether TSA is more effective in separating CO_2 than PSA and VSA processes, the calculated values of purity, regenerability, working capacity and energetic requirement for the ten different faujasite structures are plotted in Fig. 6. For comparison, moderate conditions were selected for TSA (P=100 kPa, T_{ads}=313 K, T_{des}=413 K), PSA (T=313 K, P_{ads}=1000 kPa, P_{des}=100 kPa) and VSA (T=313 K, P_{ads}=100 kPa, P_{des}=10 kPa). Fig. 6a shows that TSA presents the highest purity values for almost all the structures, followed by VSA and PSA. Even reducing the vacuum in VSA process to 5 kPa such high purity provided by TSA is not achieved. In addition, TSA is more effective in cleaning faujasites with 24 or more Al atoms per unit cell compared to PSA and VSA (see Fig. 6b), leading to a higher value of regenerability. These differences in regenerability are more pronounced in structures with high Al content, where the values obtained for PSA and VSA are extremely low. Moreover, Fig. 6c shows that TSA far surpasses PSA and VSA in

working capacity for intermediate and high Al content structures. For faujasite structures like 0-FAU to 24-FAU, with a low Henry coefficient (10^{-5} to 10^{-4} mol·kg^{-1}·Pa^{-1}), the working capacity under TSA conditions is very small (red bars in Fig. 6c). This fact requires heating up the entire sorbent to relatively high temperatures to get the capture of a small amount of CO_2, resulting in a very expensive heating cost. In this case, the energy required for heating the system is much greater than the energy required for overcoming the endothermic desorption process (*i.e.,* first and second terms in Eq. (6), respectively). Thus, materials with low Henry coefficient are not suitable for operating under TSA conditions. However, in a PSA process, these materials present high working capacities due to their low CO_2 uptake at the desorption step (*i.e.,* atmospheric pressure). On the contrary, 64-FAU to 96-FAU structures present higher Henry coefficients (around 10^{-3} mol·kg^{-1}·Pa^{-1}) due to the electrostatic interactions with the guest molecules and the Na^+ cations, resulting in much higher working capacities under TSA conditions. For these materials, it is worth investing energy in heating the system due to the large amount of CO_2 desorbed. Therefore, we expect that these results could be generalized to some extent at least for zeolite structures.

Finally, Fig. 6d shows that TSA process allows to obtain much higher values of purity, regenerability and working capacity for 64-, 77-, 88-and 96-FAU structures at a very similar energetic cost compared to P/VSA. Nevertheless, the thermal regeneration energy per ton CO_2 captured for low Al content structures is extremely high, even out of the scale, due to the poor working capacity. Therefore, although TSA process is not appropriated for low Al content faujasites, it is highly recommended against PSA and VSA for high Al content structures. To complement the study, these three processes have been also evaluated at different operative conditions. The resultant metrics for TSA, VSA and PSA (*i.e.,* purity, working capacity and thermal regeneration energy or adiabatic work) at these conditions are available in Sections V, VI and VII of the Supplementary data.

Note that for a true comparison between thermal energy and adiabatic work, it is necessary to consider a conversion coefficient, which would reduce the energetic requirements plotted for TSA.
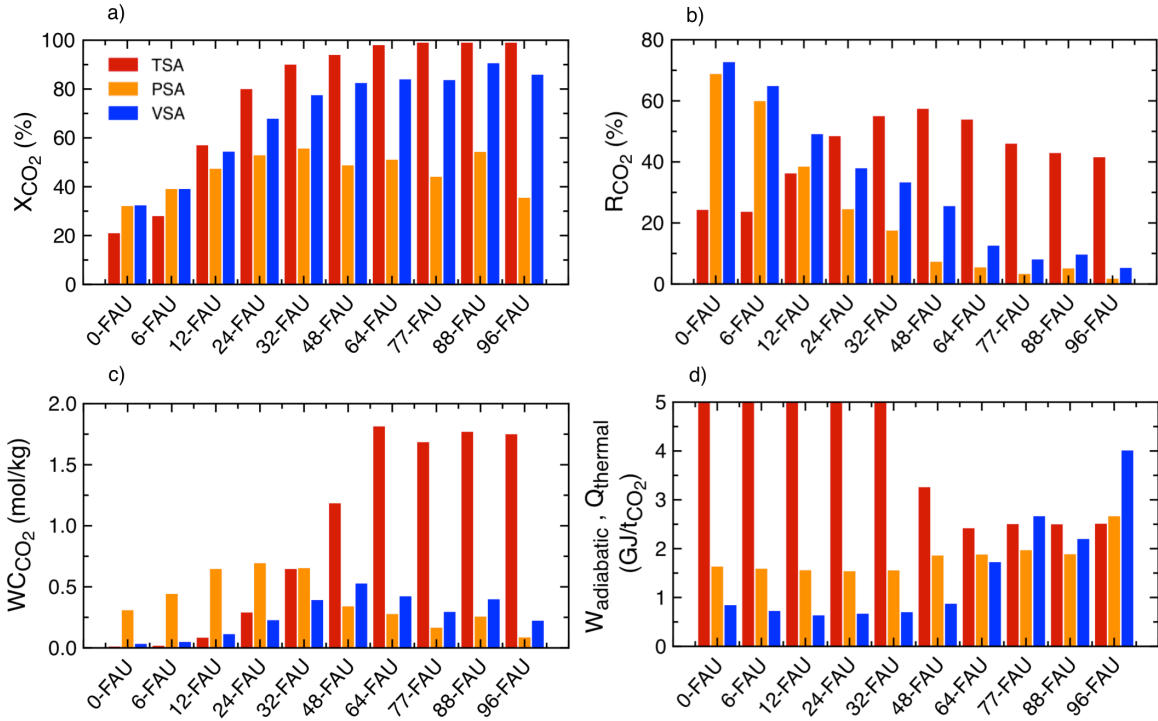
Figure 6. Comparison for a) CO_2 purity at outlet, b) regenerability, c) working capacity per cycle, and d) energetic requirement per ton CO_2 between TSA (red, T_{ads}=313 K, T_{des}=413 K), PSA (orange, T=313 K, P_{ads}=1000 kPa, P_{des}=100 kPa) and VSA (blue, T=313 K, P_{ads}=100 kPa, P_{des}=10 kPa) processes. The Y-axis in Fig. 6d represents the thermal regeneration energy (for TSA process) or the adiabatic work for expansion/compression (for VSA/PSA processes). Calculated values for PSA and VSA processes are taken from our previous work [38].

4. Conclusions

Five different evaluation criteria are considered in this work to analyze the CO_2 capture performance for each faujasite under the studied conditions: selectivity, working capacity, regenerability, purity and thermal regeneration energy, considering the difference between the uptake under adsorption and desorption conditions.

The total thermal regeneration energy is obtained considering both the energy required for heating the adsorbent material and the energy required to overcome the endothermic desorption process. To this end, the heat capacity of the adsorbent material is needed. Since only a limited number of specific heat capacities have already been measured and reported in literature for cation-exchanged faujasites, the heat capacities for all the structures were calculated by means of the oxide summation technique. The calculated heat capacities for all the structures range from 0.78-0.86 kJ/kg·K at 313 K to 0.98-1.15 kJ/kg·K at 473 K. These values are considerably lower than those conventionally employed in aqueous amine solutions, highlighting one of the main advantages of employing zeolites or other porous solid materials in TSA processes.

The 96-FAU structure presents the highest CO_2 selectivity at all the temperatures considered, ranging from 1150 (313 K) to 46 (473 K), while 0-FAU has the lowest values. Highest purities are obtained for high Al-content structures, with values above 90% for structures containing more than 48 Na^+ atoms per unit cell. Purity values corresponding to 77-FAU, 88-FAU and 96-FAU structures are coincident. Conversely, purity values for 0-FAU, 6-FAU and 12-FAU structures are very low, making them not attractive for TSA. Maximum regenerability values are obtained for intermediate Al content structures, with 48-FAU having the highest value at all temperatures explored. Even though, it should be noted that although certain structures such as 12-FAU and 24-FAU present moderately high regenerability, their uptake is so low that the amount of recovered CO_2, in absolute terms, is small.

The results for mass capacity and volumetric capacity are compared with those for promising adsorbent materials found in literature. Thus, high Al-content faujasite structures

present competitive capacity values, beating the clear majority of the other materials and being only surpassed in volumetric capacity by zeolite CaA.

The optimal desorption temperature for the ten faujasite structures evaluated varies in the range 413 – 443 K whereas the minimum value of thermal energy per ton of CO_2 recovered at 413 K is for the 64-FAU framework with a value of 2.42 GJ/tCO_2.

Comparison of present TSA results with our recent PSA and VSA ones shows that there is no structure that works well for all three processes. Thus, each process reaches optimum conditions for certain range of Al content. The best faujasite structures to be used in TSA processes for post-combustion CO_2 capture in the range 413 K – 473 K are those with a higher Al content, from 64-FAU to 96-FAU. Intermediate Al content 48-,64-FAU perform better at VSA conditions, and low Al content 12-,24-FAU structures are more suitable for PSA processes.

Moreover, at moderate operative conditions, TSA presents the highest purity values for almost all the structures, followed by VSA and PSA. Even reducing the vacuum in VSA process the TSA purity is not reached. In addition, TSA is more effective in cleaning faujasites with 24 or more Al atoms per unit cell compared to PSA and VSA leading to a higher value of regenerability. These differences in regenerability are more pronounced in structures with high Al content, where the values obtained for PSA and VSA are extremely low.

Finally, the forgoing results demonstrate that from a thermodynamic point of view, TSA processes can be an excellent choice for high Al content faujasites structures, due to the good compromise between high working capacity and moderate thermal regeneration energy. However, it should be noted that these results are based purely on equilibrium properties. Kinetic studies of diffusion coefficients and full process simulations are necessary to unequivocally determine whether TSA performance is better than V/PSA for these materials. In fact, although TSA processes are easier to implement and can benefit from the low-grade heat in a power plant as a source of energy for regeneration, the variation (swing) of temperature is much slower than the pressure change, requiring longer step times than V/PSA. Hence, further investigations need to be conducted to get more reliable predictions including kinetic effects and real flue gas conditions.

Acknowledgements

Appendix A. Supplementary data

Supplementary data associated with this article can be found, in the online version, at http://dx.doi.org/…..

Section I contains n-FAU heat capacity calculation procedure; Section II includes pure component adsorption isobars for CO_2; Section III reports the mixture adsorption isobars for CO_2 and N_2, Section IV describes the selectivities obtained from IAST calculations using pure isotherm data and Sections V, VI and VII compare the purity, the working capacity and the thermal regeneration energy or the adiabatic work, respectively at different operative conditions.

Nomenclature

BTC   Benzene-1,3,5-tricarboxylate

C ideal gas concentration at the feeding-gas conditions (kmol·m^{-3})

C_p^i heat capacity of i component (kJ·kg^{-1}· K^{-1})

CCS/U   Carbon capture and sequestration/utilization

dobpdc   4,4'-dioxidobiphenyl-3,3'-dicarboxylate

en   ethylenediamine

EOS   Equation of state

FAU   Faujasite

GC   Grand canonical

GCMC   Grand canonical Monte Carlo

IAST   Ideal adsorbed solution theory

L length of packed bed (m)

LJ   Lennard-Jones

LSX   Low silica X

LTA   Linde type A

MC   Monte Carlo

MEA   Monoethanolamine

mmen   N,N'-dimethylethylenediamine

MOF   Metal organic framework

N amount adsorbed per mass of adsorbent (mol·kg^{-1})

NIST   National Institute of Standards and Technology

$N_{k,sat}$ maximum loading (saturation) of component A (kmol·m⁻³)

P_{TOT} total initial pressure (kPa)

PSA   Pressure swing adsorption

q_i partial charge of atom i (e⁻)

q_{ST} isosteric heat of adsorption at infinite dilution (kJ·mol⁻¹)

R gas constant (8.314 kPa·m³·kmol⁻¹·K⁻¹)

r_{ij} distance between a pair of atoms i and j (m)

$S_{A/B}$ selectivity

t time (s)

T temperature (K)

TSA   Temperature swing adsorption

u superficial gas velocity (m·s⁻¹)

U_{ij} potential energy between a pair of atoms i and j (kJ·mol⁻¹)

U_g total potential energy of an isolated guest molecule (kJ·mol⁻¹)

V total volume of packed bed (m³)

VOC   Volatile Organic Compounds

VPSA   Volume Pressure Swing Adsorption

VSA   Volume Swing Adsorption

W adiabatic energy requirement for compression/vacuum (kJ)

WC working capacity of the targeted component in the mixture (mol·kg⁻¹)

x_A mole fraction of component A in the adsorbed phase

y_A mole fraction of component A in the gas (bulk) phase

z distance along the adsorber (m)

Greek symbols:

ϵ	voidage of bed
ε_{ij}	Lennard-Jones potential well depth (kJ·mol^{-1})
ε_0	vacuum permittivity (F·m^{-1})
κ	polytropic parameter of gases
η	feeding/vacuum blower efficiency
ϕ	adsorbed composition factor [adim.]
ρ_S	framework density (kg·m^{-3})
σ_{ij}	Lennard-Jones potential diameter (m)
τ	time necessary per saturation in a cycle [adim.]
μ	chemical potential (kJ·mol^{-1})
ν	intersticial gas velocity (m·s^{-1})

Suscripts:

ads/feed	adsorption or feeding conditions
des/regen	desorption or regeneration conditions
k	species in the gas mixture $(k = A, \ B, \ C, ...)$
out	mixture exiting the adsorber

References

[1] M. M. F. Hasan, E. L. First, C. A. Floudas, Cost-effective CO_2 capture based on in silico screening of zeolites and process optimization, Phys. Chem. Chem. Phys. 15 (2013) 17601-17618.

[2] N. MacDowell, N. Florin, A. Buchard, J. Hallett, A. Galindo, G. Jackson, C. S. Adjiman, C. K. Williams, N. Shah, P. Fennell, An overview of CO_2 capture technologies, Energy Environ. Sci. 3 (2010) 1645-1669.

[3] S. Chaemchuen, N. A. Kabir, K. Zhou, F. Verpoort, Metal-organic frameworks for upgrading biogas via CO_2 adsorption to biogas green energy, Chem. Soc. Rev. 42 (2013) 9304-9332.

[4] J. Wang, L. Huang, R. Yang, Z. Zhang, J. Wu, Y. Gao, Q. Wang, D. O'Hare, Z. Zhong, Recent advances in solid sorbents for CO_2 capture and new development trends, Energy Environ. Sci. 7 (2014) 3478-3518.

[5] N. Hedin, L. Andersson, L. Bergstrom, J. Yan, Adsorbents for the post-combustion capture of CO_2 using rapid temperature swing or vacuum swing adsorption, Appl. Energy 104 (2013) 418-433.

[6] S. Chu, Carbon capture and sequestration, Science 325 (2009) 1599.

[7] N. MacDowell, N. Florin, A. Buchard, J. Hallett, A. Galindo, G. Jackson, C. S. Adjiman, C. K. Williams, N. Shah, P. Fennell, An overview of CO_2 capture technologies, Energy Environ. Sci. 3 (2010) 1645-1669.

[8] Ch. Yu, Ch. Huang, C.S. Tan, A Review of CO_2 Capture by Absorption and Adsorption, Aerosol Air Qual. Res. 12 (2012) 745-769.

[9] J. D. Figueroa, T. Fout, S. Plasynski, H. McIlvried, R. D. Srivastava, Advances in CO_2 capture technology, Int. J. Greenh. Gas Control 2 (2008) 9–20.

[10] K. Sumida, D. L. Rogow, J. A. Mason, T. M. McDonald, E. D. Bloch, Z. R. Herm, T. H. Bae, J. R. Long, Carbon Dioxide Capture in Metal–Organic Frameworks, Chem. Rev. 112, (2012) 724-781.

[11] J. M. Huck, L.-Ch. Lin, A. H. Berger, M. N. Shahrak, R. L. Martin, A. S. Bhown, M. Haranczyk, K. Reuter, B. Smit, Evaluating different classes of porous materials for carbon capture, Energy Environ. Sci. 7 (2014) 4132-4146.

[12] R. Ribeiro, C. A. Grande, A.E. Rodrigues, Electric swing adsorption for gas separation and purification: a review, Sep. Sci. Technol. 49 (2014) 1985-2002.

[13] S. Sircar, Basic research needs for design of adsorptive gas separation processes, Ind. Eng. Chem. Res. 45 (2006) 5435-5448.

[14] J. A. Mason, K. Sumida, Z. R. Herm, R. Krishna, J. R. Long, Evaluating metal-organic frameworks for post-combustion carbon dioxide capture via temperature swing adsorption, Energy Environ. Sci. 4 (2011) 3030-3040.

[15] M. A. Granato, T. J. H. Vlugt, A. E. Rodrigues, Molecular simulation of propane-propylene binary adsorption equilibrium in zeolite 13X, Ind. Eng. Chem. Res. 46 (2007) 7239-7245.

[16] C. Shen, Z. Liu, P. Li, J. Yu, Two-stage VPSA process for CO_2 capture from flue gas using activated carbon beads, Ind. Eng. Chem. Res. 51 (2012) 5011-5021.

[17] M. Ishibashi, H. Ota, N. Akutsu, S. Umeda, M. Tajika, J. Izumi, A. Yasutake, T. Kabata, Y. Kageyama, Technology for removing carbon dioxide from power plant flue gas by the physical adsorption method, Energy Convers. Mgmt. 37 (1996) 929-933.

[18] J. Merel, M. Clausse, F. Meunier, Experimental investigation on CO_2 post-combustion capture by indirect thermal swing adsorption using 13X and 5A zeolites, Ind. Eng. Chem. Res. 47 (2008) 209-215.

[19] K. Z. House, C. F. Harvey, M. J. Aziz, D. P. Schrag, The energy penalty of post-combustion CO_2 capture & storage and its implications for retrofitting the U.S. installed base, Energy Environ. Sci. 2 (2009) 193.

[20] L. Lin, A. H. Berger, R. L. Martin, J. Kim, J. A. Swisher, K. Jariwala, C. H. Rycroft, A. S. Bhown, M. W. Deem, M. Haranczyk, B. Smit, In silico screening of carbon-capture materials, Nat. Mater. 11 (2012) 633-641.

[21] I. Matito-Martos, A. Martin-Calvo, J. J. Gutierrez-Sevillano, M. Haranczyk, M. Doblare, J. B. Parra, C. O. Ania, S. Calero, Zeolite screening for the separation of gas mixtures containing SO_2, CO_2 and CO, Phys. Chem. Chem. Phys. 16 (2014) 19884-19893.

[22] N. A. Rashidi, S. Yusup, An overview of activated carbons utilization for the post-combustion carbon dioxide capture, J. CO_2 Util. 13 (2016) 1-16.

[23] J. Liu, P. K. Thallapally, B. P. McGrail, D. R. Brown, J. Liu, Progress in adsorption-based CO_2 capture by metal-organic frameworks, Chem. Soc. Rev. 41 (2012) 2308-2322.

[24] Z. Zhang, Z. Z. Yao, S. Xiang, B. Chen, Perspective of microporous metal-organic frameworks for CO_2 capture and separation, Energy Environ. Sci. 7 (2014) 2868-2899.

[25] J. Ling, A. Ntiamoah, P. Xiao, D. Xu, P. A. Webley, Y. Zhai, Overview of CO_2 capture from flue gas streams by vacuum pressure swing adsorption technology, Austin J. Chem. Eng. 1 (2014) 1-7.

[26] J. A. Dunne, M. Rao, S. Sircar, R. J. Gorte, A. L. Myers, Calorimetric heats of adsorption and adsorption isotherms. 2. O_2, N_2, Ar, CO_2, CH_4, C_2H_6 and SF_6 on NaX, H-ZSM-5, and Na-ZSM-5 zeolites, Langmuir 12 (1996) 5896-5904.

[27] P. L. Llewellyn, G. Maurin, Chapter 17 – Gas adsorption in zeolites and related materials, Stud. Surf. Sci. Catal. 168 (2007) 555-610.

[28] M. Palomino, A. Corma, F. Rey, S. Valencia, New insights on CO_2-methane separation using LTA zeolites with different Si/Al ratios and a first comparison with MOFs, Langmuir 26 (2010) 1910-1917.

[29] R. Banerjee, A. Phan, B. Wang, C. Knobler, H. Furukawa, M. O'Keeffe, O. M. Yaghi, High-throughput synthesis of zeolitic imidazolale frameworks and application to CO_2 capture, Science 319 (2008) 939-943.

[30] Y. S. Bae, R. Q. Snurr, Development and evaluation of porous materials for carbon dioxide separation and capture, Angew. Chem. Int. Ed. 50 (2011) 11586-11596.

[31] Y. Li, J. Yu, New stories of zeolite structures: their descriptions, determinations, predictions, and evaluations, Chem. Rev. 14 (2014) 7268-7316.

[32] M. E. Davis, Ordered porous materials for emerging applications, Nature 417 (2002) 813-821.

[33] C. Martínez, A. Corma, Inorganic molecular sieves: preparation, modification and industrial application in catalytic processes, Coord. Chem. Rev. 255 (2011) 1558-1580.

[34] D. H. Olson, The crystal structure of dehydrated NaX, Zeolites 15 (1995) 439-443.

[35] A. Corma, From microporous to mesoporous molecular sieve materials and their use in catalysis, Chem. Rev. 97 (1997) 2373-2420.

[36] M. Eic, D.M. Ruthven, Diffusion of linear paraffins and cyclohexane in NaX and 5A zeolite crystals, Zeolites 8 (1988) 472-479.

[37] B. Smit, T. L. M. Maesen, Molecular simulations of zeolites: adsorption, diffusion, and shape selectivity, Chem. Rev. 2008, 108, 4125−4184.

[38] H. Prats, D. Bahamon, G. Alonso, X. Giménez, P. Gamallo, R. Sayós, Optimal faujasite structures for post combustion CO_2 capture and separation in different swing adsorption processes, J. CO_2 Util. 19 (2017) 100-111.

[39] W. Löwenstein, The distribution of aluminum in the tetrahedra of silicates and aluminates, Am. Mineral. 39 (1954) 92-96.

[40] S. Calero, D. Dubbeldam, R. Krishna, B. Smit, T. J. H. Vlugt, J. F. M. Denayer, J. A. Martens, T. L. M. Maesen, Understanding the role of sodium during adsorption: a force field for alkanes in sodium-exchanged faujasites, J. Am. Chem. Soc. 126 (2004) 11377-11386.

[41] A. Martin-Calvo, J. B. Parra, C. O. Ania, S. Calero, Insights on the anomalous adsorption of carbon dioxide in LTA zeolites, J. Phys. Chem. C 118 (2014) 25460-25467.

[42] A. Garcia-Sánchez, C. O. Ania, J. B. Parra, D. Dubbeldam, T. J. H. Vlugt, R. Krishna, S. Calero, Transferable force field for carbon dioxide adsorption in zeolites, J. Phys. Chem. C 113 (2009) 8814-8820.

[43] A. Martin-Calvo, J. J. Gutiérrez-Sevillano, J. B. Parra, C. O. Ania, S. Calero, Transferable force fields for adsorption of small gases in zeolites, Phys. Chem. Chem. Phys. 17 (2015) 24048-24055.

[44] S. Plimpton, Fast parallel algorithms for short-range molecular dynamics, J. Comp. Phys. 117 (1995) 1-19.

[45] D. Frenkel, B. Smit, Understanding Molecular Simulation: from Algorithms to Applications, Academic Press, London, 2002.

[46] E. J. Granite, H. W. Pennline, Photochemical removal of mercury from flue gas, Ind. Eng. Chem. Res. 41 (2002) 5470-5476.

[47] D. Y. Peng, D. B. Robinson, A new two-constant equation of state, Ind. Eng. Chem. Fundam. 15 (1976) 59-64.

[48] E. W. Lemmon, M. O. McLinden, M. L. Huber, NIST thermodynamic properties of refrigerants and refrigerants mixtures database (REFPROP), version 7.0, 2002.

[49] S. K. Shibata, S. I. Sandler, Critical evaluation of equation of state mixing rules for the prediction of high-pressure phase equilibria, Ind. Eng. Chem. Res. 28 (1989) 1893-1898.

[50] J. Vrabec, G. K. Kedia, U. Buchhauser, R. Meyer-Pittroff, H. Hasse, Thermodynamic models for vapor-liquid equilibria of nitrogen + oxygen + carbon dioxide at low temperatures, Cryogenics 49 (2009) 72-79.

[51] T. H. Bae, M. R. Hudson, J. A. Mason, W. L. Queen, J. J. Dutton, K. Sumida, K. J. Micklash, S. S. Kaye, C. M. Brown, J. R. Long, Evaluation of cation-exchanged zeolite adsorbents for post-combustion carbon dioxide capture, Energy Environ. Sci. 6 (2013) 128-138.

[52] M. Wiedt, J. P. Sculley, W. M. Verdegaal, A. A. Yakovenko, H. Zhou, Unprecedented activation CO_2 capture properties of an elastic single-molecule trap, Chem. Commun. 49 (2013) 9612-9614.

[53] J. P. Sculley, W. M. Verdegaal, W. G. Lu, M. Wriedt, H. Zhou, High-throughput analytical model to evaluate materials for temperature swing adsorption processes, Adv. Mater. 25 (2013) 3957-3961.

[54] T. J. H. Vlugt, E. García-Pérez, D. Dubbeldam, S. Ban, S. Calero, Computing the heat of adsorption using molecular simulations: the effect of strong coulombic interactions, J. Chem. Theory Comput. 4 (2008) 1107-1118.

[55] W. G. Allinson, M. T. Ho, P. R. Neal, D. E. Wiley, The methodology used for estimating the costs of CCS, Conference: 8th International Conference on Greenhouse Gas Control Technologies (GHGT-8), At Trondheim, Norway.

[56] J. Boerio-Goates, R. Stevens, B. K. Hom, B. F. Woodfield, P. M. Piccione, M. E. Davis, A. Navrotsky, Heat capacities, third-law entropies and thermodynamic functions of SiO_2 molecular sieves from T = 0 K to 400 K, J. of Chem. Therm. 34 (2002) 205-227.

[57] A. Findikakis, Heat Capacity Analysis Report, U.S. Department of Energy. November 2004. DOI: 10.2172/838658.

[58] P. Vieillard, A predictive model for the entropies and heat capacities of zeolites, Eur. J. Mineral. 22(2010) 823-836.

[59] R. H. Weiland, J. C. Dingman, D. B. Cronin, Heat capacity of aqueous monoethanolamine, diethanolamine, N-methyldiethanolamine, and N-methyldiethanolamine-based blends with carbon dioxide, J. Chem. Eng. Data 42 (1997) 1004-1006

[60] C. W. Skarstrom, Method and apparatus for fractionating gaseous mixtures by adsorption, US Patent 2944627 A, 1960.

[61] M. Khurana, S. Farooq, Adsorbent screening for post-combustion carbon capture: a method relating equilibrium isotherm characteristics to optimum VSA process performance, Ind. Eng. Chem. Res. 55 (2016) 2447-2460.

[62] A. K. Rajagopalan, A. M. Avila, A. Rajendran, Do adsorbent screening metrics predict process performance? A process optimization based study for post-combustion capture of CO_2, Int. J. Greenh. Gas Control 46 (2016) 76-85.

[63] H. Huang, W. Zhang, D. Liu, B. Liu, G. Chen, C. Zhong, Effect of temperature on gas adsorption and separation in ZIF-8: A combined experimental and molecular simulation study, Chem. Eng. Sci. 66 (2011) 6297-6305.

[64] W. R. Lee, S. Y. Hwang, D. W. Ryu, K. S. Lim, S. S. Han, D. Moon, J. Choide, C. S. Hong, Diamine-functionalized metal-organic framework: exceptionally high CO_2 capacities from ambient air and flue gas, ultrafast CO_2 uptake rate, and adsorption mechanism, Energy Environ. Sci. 7 (2014) 744-751.

[65] T. M. McDonald, J. A. Mason, X. Kong, E. D. Bloch, D. Gygi, A. Dani, V. Crocellà, F. Giordanino, S. O. Odoh, W. S. Drisdell, B. Vlaisavljevich, A. L. Dzubak, R. Poloni, S. K. Schnell, N. Planas, K. Lee, T. Pascal, L. F. Wan, D. Prendergast, J. B. Neaton, B. Smit, J. B. Kortright, L. Gagliardi, S. Bordiga, J. A. Reimer, J. R. Long, Cooperative insertion of CO_2 in diamine-appended metal-organic frameworks, Nature 519 (2015) 303-308.

[66] M. Zaman, J. H. Lee, Carbon capture from stationary power generation sources: A review of the current status of the technologies, Korean J. Chem. Eng. 30 (2013) 1794-1526.